

Enhanced triacylglycerol catabolism by Carboxylesterase 1 promotes aggressive colorectal carcinoma

Daria Capece, ... , Gabriele Cruciani, Guido Franzoso

J Clin Invest. 2021. <https://doi.org/10.1172/JCI137845>.

Research In-Press Preview Metabolism Oncology

The ability to adapt to low-nutrient microenvironments is essential for tumor-cell survival and progression in solid cancers, such as colorectal carcinoma (CRC). Signaling by the NF- κ B transcription-factor pathway associates with advanced disease stages and shorter survival in CRC patients. NF- κ B has been shown to drive tumor-promoting inflammation, cancer-cell survival and intestinal epithelial cell (IEC) dedifferentiation in mouse models of CRC. However, whether NF- κ B affects the metabolic adaptations that fuel aggressive disease in CRC patients is unknown. Here, we identified carboxylesterase 1 (CES1) as an essential NF- κ B-regulated lipase linking obesity-associated inflammation with fat metabolism and adaptation to energy stress in aggressive CRC. CES1 promoted CRC-cell survival via cell-autonomous mechanisms that fuel fatty-acid oxidation (FAO) and prevent the toxic build-up of triacylglycerols. We found that elevated CES1 expression correlated with worse outcomes in overweight CRC patients. Accordingly, NF- κ B drove CES1 expression in CRC consensus molecular subtype (CMS)4, associated with obesity, stemness and inflammation. CES1 was also upregulated by gene amplifications of its transcriptional regulator, *HNF4A*, in CMS2 tumors, reinforcing its clinical relevance as a driver of CRC. This subtype-based distribution and unfavourable prognostic correlation distinguished CES1 from other intracellular triacylglycerol lipases and suggest CES1 could provide a route to treat aggressive CRC.

Find the latest version:

<https://jci.me/137845/pdf>



Enhanced triacylglycerol catabolism by Carboxylesterase 1 promotes aggressive colorectal carcinoma

Daria Capece^{1,2,#,*}, Daniel D'Andrea^{1,3,#}, Federica Begalli¹, Laura Goracci⁴, Laura Tornatore¹, James L. Alexander⁵, Alessandra Di Veroli⁴, Shi-Chi Leow^{6,7}, Thamil S. Vaiyapuri⁸, James K. Ellis^{1,9}, Daniela Verzella¹, Jason Bennett¹, Luca Savino^{1,10}, Yue Ma⁵, James McKenzie⁹, Maria Luisa Doria⁹, Sam Mason⁹, Kern Rei Chng¹¹, Hector C. Keun⁹, Gary Frost⁵, Vinay Tergaonkar⁸, Katarzyna Broniowska¹², Walter Stunkel^{6,13}, Zoltan Takats⁹, James Kinross⁹, Gabriele Cruciani⁴ and Guido Franzoso^{1,*}

¹Department of Immunology and Inflammation, Imperial College London, London W12 0NN, UK.

²Department of Biotechnological and Applied Clinical Sciences (DISCAB), University of L'Aquila, 67100 L'Aquila, Italy.

³Current address: MRC centre for Neuropsychiatric Genetics and Genomics, Cardiff University, Cardiff CF24 4HQ, UK.

⁴Department of Chemistry, Biology and Biotechnology, University of Perugia, 06123 Perugia, Italy.

⁵Department of Department of Metabolism, Digestion and Reproduction, Imperial College London, London W12 0NN, UK.

⁶Singapore Institute for Clinical Sciences (SICS), Agency for Science Technology and Research (A*STAR), Singapore, Singapore 117609.

⁷Current address: Agency for Science, Technology and Research (A*STAR), Singapore, Singapore 138668.

⁸Institute of Molecular and Cell Biology (IMCB), A*STAR (Agency for Science, Technology and Research), 138673, Singapore

⁹Department of Surgery and Cancer, Imperial College London, London SW7 2AZ, UK.

¹⁰Department of Medical, Oral, and Biotechnological Sciences, "G. D'Annunzio" University of Chieti-Pescara, 66100, Chieti, Italy.

¹¹Genome Institute of Singapore, Singapore, Singapore 138672.

¹²Metabolon, Inc., Morrisville, NC.

¹³Current address: Rhea Pharmaceutical Sciences Pte Ltd, 16, Gemmill Lane, Singapore 0699264

#Joint first author

*Corresponding author

Correspondence:

Guido Franzoso,
Imperial College London, CWB
Du Cane Road, W12 0NN, London UK
g.franzoso@imperial.ac.uk
+44 (0)20 3313 8421

Daria Capece,
Imperial College London, CWB
Du Cane Road, W12 0NN, London UK
d.capece@imperial.ac.uk
+44 (0)20 8383 8430

CONFLICT OF INTEREST

The authors have declared that no conflict of interest exists.

ABSTRACT

The ability to adapt to low-nutrient microenvironments is essential for tumor-cell survival and progression in solid cancers, such as colorectal carcinoma (CRC). Signaling by the NF- κ B transcription-factor pathway associates with advanced disease stages and shorter survival in CRC patients. NF- κ B has been shown to drive tumor-promoting inflammation, cancer-cell survival and intestinal epithelial cell (IEC) dedifferentiation in mouse models of CRC. However, whether NF- κ B affects the metabolic adaptations that fuel aggressive disease in CRC patients is unknown. Here, we identified carboxylesterase 1 (CES1) as an essential NF- κ B-regulated lipase linking obesity-associated inflammation with fat metabolism and adaptation to energy stress in aggressive CRC. CES1 promoted CRC-cell survival via cell-autonomous mechanisms that fuel fatty-acid oxidation (FAO) and prevent the toxic build-up of triacylglycerols. We found that elevated CES1 expression correlated with worse outcomes in overweight CRC patients. Accordingly, NF- κ B drove CES1 expression in CRC consensus molecular subtype (CMS)4, associated with obesity, stemness and inflammation. CES1 was also upregulated by gene amplifications of its transcriptional regulator, *HNF4A*, in CMS2 tumors, reinforcing its clinical relevance as a driver of CRC. This subtype-based distribution and unfavourable prognostic correlation distinguished CES1 from other intracellular triacylglycerol lipases and suggest CES1 could provide a route to treat aggressive CRC.

KEYWORDS: NF- κ B; CES1; HNF4A; lipid metabolism; colorectal cancer.

INTRODUCTION

Tumor cells must adapt to the low nutrient concentrations in the tumor microenvironment (TME) in order to survive, proliferate and spread to distant sites (1-4). The availability of nutrients, such as glucose, is generally lower in solid tumors than normal tissues, due to the higher metabolic requirements of rapidly proliferating tumor cells and the inadequate blood supply by the abnormal and inefficient tumor vasculature (5, 6). This poses a major metabolic challenge for tumor cells, exacerbated by the presence of driver mutations that commit these cells to a biosynthetic metabolic programme, while restricting their capacity to respond to metabolic stress (2, 3). Tumor cell clones that are able to meet this challenge have a significant growth advantage and greater metabolic adaptability, which fuel malignant progression, epithelial to mesenchymal transition (EMT), and metastatic spread (4, 7).

Several adaptive metabolic mechanisms have been described in colorectal carcinoma (CRC) (8-12). Early studies have shown that glucose deprivation drives the acquisition of RAS-pathway mutations, which promote CRC-cell adaptation to low glucose availability in part by increasing glucose uptake through the upregulation of *Glucose Transporter 1 (GLUT1)* (8). Subsequent studies have reported additional metabolic responses of CRC cells to starvation, including glucose deprivation-induced MYC stabilization, which enhances glycolytic flux by upregulating *GLUT1* and other glycolysis-associated genes (9, 10), and alterations in the expression of genes involved in glutamine metabolism (11, 12). Recent reports have shown that metabolic adaptations also play an important role in the EMT and metastatic dissemination, which requires CRC cells to migrate through and adapt to diverse metabolic tumor environments, both upon entering the circulation and colonising distal sites (4, 7, 13, 14). Strong evidence also indicates that an upregulation of oxidative metabolism and fatty acid oxidation (FAO) during energy stress is essential for EMT, metastatic spread, and therapy resistance in many cancer types, including CRC (15-17). However, the precise mechanisms underpinning this metabolic

plasticity of cancer cells and its influence on tumor behavior and clinical outcomes in CRC patients remain poorly understood.

NF- κ B transcription factors are central regulators of immunity and inflammation (18). They are also major drivers of oncogenesis, disease recurrence, and therapy resistance, owing to their capacity to upregulate genes that suppress cancer-cell apoptosis and orchestrate inflammation in the TME (18, 19). Studies in mouse models of CRC have demonstrated an essential role for NF- κ B in both tumor initiation and progression (20, 21). During CRC initiation, NF- κ B signaling enhances WNT/ β -catenin activation and stemness in intestinal epithelial cells (IEC) (20); whereas in established tumors, NF- κ B mediates a crucial link between malignancy and inflammation by stimulating tumor-promoting inflammation and the survival of intestinal tumor cells (21). Other reports have implicated NF- κ B signaling in the regulation of energy metabolism, metabolic stress adaptation, and EMT in both models of inflammation and cancer, including CRC (18, 22-28). In keeping with these findings, several clinical studies have identified a correlation between higher NF- κ B activity and shorter overall survival (OS), as well as more advanced disease stages, in CRC patients (29-32). However, the paucity of the molecular clinical investigations has limited the mechanistic understanding of the pathogenic relationship of NF- κ B signaling with tumor phenotype and clinical evolution in CRC. Consequently, precisely how NF- κ B activation drives aggressive disease progression in CRC patients remains poorly understood.

The consensus molecular subtype (CMS) classification of CRC recently provided a robust molecular subtyping system for CRC and an important new tool for deciphering how NF- κ B impacts CRC evolution and clinical outcomes (33). Thus, we sought to interrogate this classification system as a starting point to investigate whether and how NF- κ B activity relates to intrinsic core biologic underpinnings of human CRC and features previously associated with NF- κ B-driven colorectal tumors in mouse models. We reasoned that this approach might reveal novel core cancer-cell vulnerabilities that could provide better treatments for CRC patients who are affected by hard-to-treat forms of the disease. Using

this approach, we identify carboxylesterase 1 (CES1) as an essential NF- κ B-regulated lipase promoting cancer-cell survival and adaptation to energy stress conditions in aggressive CRC. We find that elevated CES1 expression correlates with worse prognosis in overweight CRC patients and is enriched downstream of NF- κ B in mesenchymal consensus molecular subtype (CMS)4, associated with stemness, obesity, and inflammation. Our results uncover a metabolic oncogenic pathway that is mediated by NF- κ B via CES1-dependent lipid catabolism, revealing an intriguing association of NF- κ B signaling and inflammation with obesity, fat catabolism and metabolic adaptation in aggressive CMS4 tumors. These results underscore the clinical relevance of CES1 as a central driver of CRC and suggest CES1 could provide an effective route to treat CRC patients with particularly poor prognosis.

RESULTS

Inflammation and increased NF- κ B activity co-segregate with the aggressive mesenchymal CMS4 subtype

Our analysis of human datasets demonstrated that the NF- κ B activation and inflammatory gene signatures are significantly upregulated in the mesenchymal CMS4 subtype of CRC (Figure 1A; Figure 1B), associated with stemness, EMT, TGF β activation, and shorter OS and relapse-free survival (33). This finding is consistent with the reported correlation between enhanced NF- κ B activity and worse clinical outcomes in CRC patients (29-32). CMS4 tumors also exhibited a distinctive pattern of metabolic gene expression compared to other CRC subtypes (Figure 1C). Since NF- κ B is a transcriptional regulator of cell metabolism, in addition to being a central regulator of inflammation and the EMT (18, 19, 22-28), this suggested that increased NF- κ B activation could contribute to the distinct metabolic features of CMS4 tumors.

NF- κ B inhibition markedly disrupts lipid metabolism under energy stress conditions

To test this hypothesis, while excluding any potential confounding effects resulting from the idiosyncratic metabolic dependencies of cancer cells, we investigated the global impact of NF- κ B inhibition on the metabolism of non-transformed mouse embryonic fibroblasts (MEFs) cultured under low glucose conditions (24), mimicking the low-glucose concentrations present in the tumor microenvironment (TME) (5, 6). As shown in Figure S1A-S1C, RNA interference (RNAi)-mediated inhibition of the dominant NF- κ B subunit, RelA (18, 20, 34), altered the cellular abundance of over 430 metabolites, assessed by mass spectrometry (MS), before and/or after glucose limitation (GL) (Table S1). An enrichment analysis of these metabolites identified Fatty Acid Metabolism, Glycerolipid Metabolism, and Lipid Signaling as the metabolic classes that were most significantly altered by RelA inhibition over time (Figure 1D).

To determine in more detail the impact of NF- κ B-dependent gene transcription on lipid metabolism and its possible involvement in the adaptation to low-glucose availability, we conducted an additional profiling of 1,028 lipid species, using MEFs. As shown in Figure 1E, NF- κ B/RelA knockdown affected metabolic species from multiple lipid classes, including phospholipids, lysophospholipids and ceramides (Table S1). However, the most profound effect of RelA inhibition was a significant enrichment of TAGs and, to a lesser extent, cholesteryl esters (CEs), with a marked accumulation of several TAG and CE species during GL. RelA depletion by RNAi similarly altered lipid metabolism in the CT-26 CRC cell line, resulting in an increased cellular content of both TAGs and CEs, upon GL, and a lesser alteration of other lipid species, such as phosphocholines (Figure 2A-2C, Figure S2A, Table S1) (35). The observed effects of RelA depletion on phospholipids and ceramides were in keeping with the NF- κ B-dependent regulation of enzymes involved in inflammatory and stress-related lipid signaling, such as phospholipase A2 (36). However, the marked

alteration of TAG and CE metabolism seen in RelA-deficient cells was not expected and suggested that NF- κ B enhances lipolysis or reduces neutral lipid synthesis during low-glucose availability. To distinguish between these possibilities, we performed pulse-chase experiments using [13 C]-oleate and specific drug inhibitors to selectively block TAG hydrolysis or free-fatty acid (FFA) re-esterification. Interestingly, RNAi-mediated RelA inhibition had no effect on the rate of [13 C]-oleate incorporation into TAGs in CT-26 cells, indicating that NF- κ B does not affect TAG synthesis or FFA cellular uptake (Figure 2D, Table S1). In contrast, RelA deficiency markedly reduced TAG turnover during GL (Figure 2E, Table S1), suggesting that NF- κ B accelerates lipolysis.

NF- κ B promotes energy homeostasis and CRC cell survival by increasing oxidative FFA metabolism during starvation

Cancer cells must adapt to low-glucose availability to survive in the poorly vascularised TME (1-4, 37). Thus, we investigated whether NF- κ B-driven TAG catabolism could contribute to the metabolic adaptation of CRC cells to GL, as TAGs derived from lipid droplets are the preferred energy substrates used by cells under metabolic stress conditions (3, 38). RelA inhibition markedly diminished CT-26-cell survival during GL (Figure S2B), in keeping with previous studies (24). However, treatment with BSA-bound oleate, which circumvents the requirement for lipolysis, completely rescued RelA-deficient cells from GL-induced death (Figure 2F). Furthermore, the cytotoxic effect of RelA depletion was recapitulated by the FAO inhibitor, etomoxir, suggesting a role for FAO in the pro-survival function of NF- κ B under GL (Figure 2F).

To clarify in more detail the mechanism by which NF- κ B promotes cell survival during GL, we compared the mitochondrial bioenergetic profiles of RelA-deficient and control CT-26 cells. Notably, spare respiratory capacity (SRC), which reflects the respiratory reserve available for ATP production to support cell survival during energy stress conditions (39),

was significantly reduced by RelA inhibition (Figure 2G, Figure S2C). Treatment with etomoxir similarly diminished SRC in CT-26 cells, abrogating the difference seen between RelA-deficient and control cells (Figure 2G, Figure S2C). Mitochondrial ATP production was correspondingly impaired by the silencing of RelA (Figure 2H, Figure S2D). Conversely, oleate supplementation reversed both the reduced mitochondrial ATP production rate and the reduced SRC observed in RelA-depleted cells. Together, these data demonstrate the importance of lipolysis in NF- κ B-dependent metabolic homeostasis under GL conditions, while excluding a direct role for NF- κ B in the modulation of FFA mitochondrial import or FAO (Figure 2G-2H). We concluded that RelA deficiency reduces FFA availability for FAO and oxidative phosphorylation (OXPHOS) by impairing TAG hydrolysis under energy stress conditions, resulting in a metabolic crisis and cell death.

CES1 is a pivotal mediator of the effects of NF- κ B on lipid catabolism

To understand how NF- κ B-dependent gene transcription regulated TAG catabolism, we analysed the gene-expression profile of RelA-deficient and control MEFs, at baseline and under GL, by using RNA sequencing. Among the 1,792 metabolic genes listed in the Reactome database, we isolated the top seven genes that were most markedly downregulated by RelA deficiency at all time points investigated (Figure 3A, Figure S3A, Table S2). Notably, one of the genes in this group encoded carboxylesterase 1d (*Ces1d*), the murine ortholog of human CES1 (also known as Triacylglycerol Hydrolase), a TAG and CE lipase predominantly expressed in liver, adipose tissue, intestine and lung (40). We confirmed by qRT-PCR that *Ces1d* transcripts were strongly upregulated by GL in control MEFs, but only weakly in RelA-deficient MEFs (Figure S3B), indicating that *Ces1d* expression depends on NF- κ B. The basal expression and upregulation of *Ces1d* transcript and protein levels in CT-26 CRC cells under GL also required NF- κ B, as shown by RelA knockdown (Figure 3B-3C). Consistent with these results, RelA depletion by RNAi ablated

Ces1d hydrolase activity, assessed by using a serine esterase activity-based probe (41), thus establishing the importance of NF- κ B in promoting the Ces1d enzymatic function in CRC cells (Figure 3D). In contrast, NF- κ B had no effect on Ser660-specific phosphorylation of hormone-sensitive lipase (Hsl) (Figure S3C). Chromatin immunoprecipitation identified at least ten NF- κ B/RelA-binding (κ B) DNA elements in the promoter and intronic regions of the *Ces1d* gene (Figure S3D). These DNA elements were frequently occupied by RelA-containing NF- κ B complexes at baseline, and their occupancy by NF- κ B invariably increased upon GL (Figure 3E, Figure S3E). Luciferase assays and mutational DNA analyses confirmed the functional relevance of at least six of these κ B elements for *CES1* transcription (Figure S3F-S3G). Thus, Ces1d expression is under direct NF- κ B-dependent transcriptional control in CRC cells, both under basal and metabolic stress conditions.

Since Ces1d/CES1 specifically hydrolyses TAGs and CEs (40), we investigated whether it mediated any of the metabolic effects of NF- κ B in CRC cells. Upon Ces1d depletion, CT-26 cells exhibited a marked accumulation of TAGs and CEs, but not PCs, both at baseline and under GL (Figure 4A-4C, Figure S4A, Table S1), mimicking the effects of RelA deficiency on lipid metabolism. However, Ces1d knockdown appeared to impact neutral lipids more promptly and conspicuously than the silencing of RelA (see also Figure 2A and Figure 2C), suggesting that other genes could mitigate the metabolic effects of RelA deficiency. In pulse-chase labelling experiments using [13 C]-oleate, TAG turnover was markedly reduced in Ces1d-deficient compared to control CT-26 cells (Figure 4D, Table S1), and again this effect was more pronounced than that seen in RelA-depleted cells (see Figure 2E). Thus, we investigated whether Ces1d/CES1 could contribute to NF- κ B-dependent metabolic adaptation to energy stress conditions. As shown in Figure 4E, the silencing of Ces1d markedly diminished CT-26-cell survival following GL. Similar results were obtained using two alternative Ces1d-targeting hairpins (Ces1d #2 and Ces1d #3; Figure S4B-S4C), the structurally distinct Ces1d/CES1 inhibitors, GR-148672X (42) and WWL113 (41) (Figure 4F; Figure S4D-S4E), or MEFs (Figure S4F). Reciprocally, ectopic

Ces1d expression effectively rescued RelA-deficient cells from GL-induced death (Figure 4G, Figure S4G), mimicking the protective effect of oleate supplementation (Figure 2F). Moreover, a silencing-resistant, but not a wild-type Ces1d-encoding lentivirus reversed GL-induced death in Ces1d-depleted CT-26 cells, thus excluding any off-target effects of the Ces1d-targeting hairpins (Figure S4H-S4I). Thus, Ces1d/CES1 mediates many of the metabolic effects of RelA on lipid catabolism and is both required and sufficient to compensate for RelA loss in controlling the response of CRC cells to starvation.

CES1 depletion impairs metabolic adaptation by reducing oxidative energy metabolism and enhancing toxic TAG accumulation

Given the essential role of Ces1d/CES1 in the NF- κ B-dependent regulation of lipid catabolism and CRC cell survival during starvation, we sought to characterize the bioenergetic profile of Ces1d-deficient cells. As with etomoxir treatment, Ces1d knockdown ablated SRC in CT-26 cells, while oleate supplementation completely reversed this effect (Figure 4H, Figure S4J), in keeping with our findings in RelA-deficient CRC cells (Figure 2G). Ces1d depletion also diminished the mitochondrial ATP production rate (Figure 4I; Figure S4K). Surprisingly, however, oleate supplementation failed to rescue this impaired mitochondrial ATP production in Ces1d-depleted cells (Figure 4I, Figure S4K). Since marked TAG accumulation was shown to induce ROS formation and mitochondrial damage, leading to cell death (43), we considered whether these events could contribute to the mitochondrial dysfunction observed in Ces1d-deficient cells during GL. Indeed, Ces1d inhibition increased both non-mitochondrial respiration and ROS production in CT-26 cells, with a corresponding depletion of cellular reduced glutathione (GSH) levels (Figure 4J-4L, Figure S4J; see also Figure S4L-S4M). Comparable results were obtained using spectrophotometric methods to assess ROS and GSH levels (Figure S4N-S4O). The increase in ROS formation induced by Ces1d depletion was associated with enhanced lipid

peroxidation, which results in ferroptosis, assessed by using BODIPYTM 581/591 C11 and examining 4-hydroxynonenal (HNE)-protein adducts, a major end-product of polyunsaturated fatty acid (PUFA) peroxidation (Figure 4M, Figure S4P-S4Q) (44-47). This increased lipid peroxidation in Ces1d-deficient cells was accompanied by a depletion of glutathione peroxidase (Gpx)4 levels, another hallmark of ferroptosis (Figure S4R) (46, 48). Interestingly, enhanced ROS formation further correlated with a significant decrease of the mitochondrial membrane potential ($\Delta\Psi_m$) and a corresponding increase of the number of apoptotic cells upon Ces1d depletion, as shown by annexin V staining, TUNEL assays and the assessment of caspase-3/7 activity and nucleosomal DNA fragmentation (Figure 4N-4P, Figure S4S-S4W) (44). These data suggest that ROS accumulation in Ces1d-deficient cells results in the induction of both the ferroptosis and apoptosis pathways of cell death during GL.

We reasoned that the cytotoxic effects of exaggerated TAG accumulation could explain the failure of oleate supplementation to reverse the reduced mitochondrial ATP production rate seen in Ces1d-deficient cells (Figure 4I). Consistent with this idea, the effect of Ces1d depletion on the survival of starved CRC cells was only partly recapitulated by treatment with etomoxir (Figure S4X). Moreover, oleate supplementation failed to protect Ces1d-deficient cells from GL-induced toxicity (Figure 4Q). In contrast, the addition of Ferrostatin-1 and z-VAD-fmk, which block ferroptosis and apoptosis, respectively, together with oleate, completely rescued Ces1d-depleted CRC cells from GL-induced death (Figure 4Q; see also Figure S4X). Instead, ferrostatin-1 or z-VAD-fmk either alone or in combination, but without oleate, could only partly reverse GL-induced toxicity in Ces1d-deficient cells (Figure S4X). Collectively, these results suggest that the NF- κ B-dependent upregulation of Ces1d/CES1 mediates two important cytoprotective functions in CRC cells during metabolic stress: First, to maintain ATP homeostasis and thus enable cells to meet their energy demand by increasing the FFA supply to fuel FAO and OXPHOS; second, to

prevent the toxic build-up of neutral lipids that results in ROS production and mitochondrial damage, triggering apoptosis and ferroptosis (43).

CES1 expression portends worse clinical outcomes in overweight CRC patients

The maintenance of energy homeostasis is essential for malignant cell survival in the nutrient insufficient TME (1-4). We therefore investigated whether CES1-dependent TAG catabolism could contribute to the pathogenesis of CRC, since FAO is also involved in stem-cell renewal, anchorage independent growth and metastatic spread (15-17). 59 CRC patients were stratified on the basis of tumor-associated *CES1* expression, and the lipid composition of their tumors was analysed by MS. These analyses showed that elevated *CES1* expression correlated with a reduced abundance of multiple TAG species in the tumor tissue, compared with tumors exhibiting low *CES1* mRNA expression (Figure 5A, Figure S5A-S5B), consistent with our findings in CRC cell lines (Figure 4A). In the same CRC patient cohort, elevated *CES1* expression also correlated with shorter disease-specific survival (DSS; Figure 5B), and, interestingly, this correlation demonstrated an increased significance in overweight patients (Figure 5C). Notably, we found no prognostic correlation with *CES1* expression in the non-overweight CRC patient subgroup (Figure 5C). Similar results, demonstrating a significant association between elevated *CES1* expression and both shorter progression-free interval (PFI) and shorter DSS in overweight, but not non-overweight patients, were obtained upon analysis of an external CRC dataset from The Cancer Genome Atlas (TCGA) network using 25th percentile as cut-off value for *CES1* expression (49) (Figure 5D-5E; Figure S5C-S5D). Together, these results identify *CES1* as a hallmark of aggressive disease in overweight CRC patients.

Since obesity is a major risk factor for CRC and increases both the disease recurrence and mortality rates in CRC patients (50-52), we sought to investigate in more

detail its association with CES1 expression. Interestingly, the analysis of CRC datasets demonstrated that the obesity gene signature and percentage of overweight patients were both significantly increased in the mesenchymal CMS4 subtype, compared to other CRC subtypes (Figure 5F-5G, Figure S5E-S5F). Notably, *CES1* expression was correspondingly upregulated in the aggressive CMS4 subtype, in keeping with our findings of a correlation between CES1 expression and worse prognosis in CRC (Figure 5H; Figure S5G). Of note, CES1 expression was also upregulated in the canonical CMS2 CRC subtype (discussed below). Thus, our analyses of human datasets (33) demonstrated a clear stratification of *CES1* expression with clinically relevant core molecular subtypes of CRC, obesity-related inflammation, and patient outcome. Notably, no other intracellular TAG lipase displayed such a distinctive CRC subtype-based distribution, nor a correlation with reduced survival in CRC patients (Figure S5H-S5R). Together, these findings suggest a unique role for CES1 in the pathogenesis of aggressive CRC.

Elevated CES1 expression is driven by NF- κ B activation in CMS4 CRC and by *HNF4A* amplifications in CMS2 CRC

The high *CES1* expression observed in CMS4 CRCs was consistent with the elevated NF- κ B-activation and inflammatory gene signatures characteristic of these tumors. However, the increased *CES1* expression seen in the CMS2 subtype was unexpected, since this subtype is not linked to inflammation nor NF- κ B activation (Figure 5H). We considered that CMS2 CRCs are enriched in amplifications of the gene encoding the transcription factor, Hepatocyte Nuclear Factor 4 α (*HNF4 α*) (33), residing in the chromosome 20q11-q13 amplicon, which correlates with worse clinical outcomes in CRC patients (49, 53). Since *HNF4 α* is a transcriptional regulator of *CES1* (54), this raised the possibility that increased *CES1* expression in CMS2 CRCs could be driven by *HNF4A* amplifications. Consistent with this idea, *HNF4A* was expressed at significantly higher levels in the CMS2 than other CRC

subtypes (Figure 5I; Figure S5S). Moreover, *CES1* expression correlated with the presence of *HNF4A* amplifications, as well as *HNF4A* mRNA expression in CRC datasets (Figure S5T-S5U). Interestingly, *CES1* expression in human CRCs also correlated with the NF- κ B target-gene signature (Figure S5V), which is upregulated in the CMS4 subtype along with *CES1* (Figure 1A, Figure 5H).

These analyses of CRC patients suggested that elevated *CES1* expression is largely driven by NF- κ B activation in the CMS4 subtype and by *HNF4A* amplifications in the CMS2 subtype, underscoring the importance of *CES1* upregulation in the etiopathogenesis of CRC. Consistent with this idea, NF- κ B/RelA was activated by GL-induced Ser536 phosphorylation in three out of six human CRC cell lines evaluated (Figure S6A). Accordingly, RelA knockdown decreased *CES1* expression, resulting in TAG and CE, but not PC accumulation and impaired metabolic adaptation during energy stress only in the three CRC cell lines in which NF- κ B was activated by GL (Figure 6A-6C, Figure S6A-S6C). Strikingly, despite this cell-selective NF- κ B activation, all six CRC cell lines depended on *CES1* expression for survival during GL, as shown by the marked toxicity produced by *CES1* deficiency in starved CRC cells (Figure 6C). Similar results were obtained using two independent *CES1*-targeting hairpins (*CES1* #2 and *CES1* #3; Figure S6D-S6E). These data suggested that *CES1* is the dominant effector of NF- κ B-dependent metabolic homeostasis in CRC cells during GL, because RelA knockdown had no effect on CRC-cell survival under energy stress conditions, unless it resulted in a decrease of *CES1* expression (Figure 6A, Figure S6C). In contrast, *HNF4A* expression was higher in the RelA-independent than RelA-dependent CRC cell lines (Figure S6F), and, correspondingly, *HNF4A* knockdown diminished constitutive *CES1* expression in the three RelA-independent, but not the RelA-dependent CRC cell lines (Figure 6D; Figure S6G). Two alternative *HNF4A*-targeting hairpins produced similar effects (Figure S6G). Collectively, our results support the hypothesis that *CES1* transcription is reciprocally controlled by NF- κ B and *HNF4A* in distinct subsets of CRC.

CES1 is a potentially actionable therapeutic target in aggressive CRC

Given the profound effect of CES1 depletion on CRC-cell survival upon GL and the clinical relevance of CES1 expression in CRC pathogenesis, we hypothesised that blockade of the CES1 catalytic activity could provide an effective therapeutic strategy to treat patients with aggressive forms of CRC. In support of this hypothesis, treatment with the CES1 inhibitor, GR148672X (42), significantly increased GL-induced cell death in all human CRC cell lines investigated, while demonstrating no overt toxicity under normal culture conditions (Figure 6E, Figure S6H). Similar results were obtained using a second CES1 inhibitor (WWL113; Figure S6I-S6J) (41). These results indicated that the effects of CES1 knockdown on CRC cell survival after GL were due to reduced CES1 enzymatic activity, rather than impaired CES1 adaptor function. These findings also confirmed the contextual specificity of the CES1-targeting approach for metabolic stress conditions. Interestingly, in a mouse allograft model of CRC, treatment with GR148672X over a 10-day period significantly reduced tumor growth, with no apparent adverse effects (Figure 7A-7B, Figure S7A). At the endpoint, all control mice had developed large tumors, while mice treated with GR148672X displayed a significant reduction of both tumor volume and weight (Figure 7B-7D). Similar results, showing a marked drug-dependent inhibition of CRC oncogenesis, with no apparent toxicities, were obtained with GR148672X in a second mouse xenograft model of CRC, using the human cell line, HCT-116 (Figure 7E-7H, Figure S7B). These results are broadly consistent with a previous study, which reported a significantly reduced growth of B-cell tumors in *Ces1d*-deficient mice (55). Collectively, these data identify CES1 as a potentially actionable therapeutic target in aggressive core CRC subtypes and support the therapeutic potential of blocking CES1 to counter colorectal carcinogenesis.

DISCUSSION

Our findings uncover a metabolic mechanism mediated by CES1 that drives CRC pathogenesis downstream of inflammatory NF- κ B signaling and *HNF4A* amplification in the CMS4 and CMS2 subtypes, respectively. CES1 enhances CRC-cell survival under energy stress conditions by cell-autonomously increasing FFA availability for ATP production and preventing TAG-induced cytotoxicity mediated by ROS and phospholipid peroxidation (Figure 7I). Our results also provide a mechanism for the role of NF- κ B in the etiopathogenesis of CRC, revealing an intriguing association that links NF- κ B activity and inflammation with obesity and fat metabolism in the mesenchymal CMS4 subtype. Further, our data provide a basis for the pathogenic role of prognostically unfavourable *HNF4A* gene amplifications in CRC patients (53). Thus, despite utilizing entirely different, genetic and inflammatory oncogenic pathways, respectively, CMS2 and CMS4 tumors both rely on the same CES1-mediated downstream mechanism to withstand starvation and drive malignant CRC evolution. Future studies will clarify the precise mechanisms for the *CES1* transcriptional regulation by NF- κ B and HNF4 α in human CRC. Notwithstanding, our results underscore the central metabolic role of CES1 in CRC etiopathogenesis.

Strong epidemiological evidence demonstrates that the recurrence and mortality rates of CRC patients markedly increase in obese people, underscoring the importance of lipid metabolism in CRC pathogenesis (50-52). A prominent feature of CRC in obese patients is a chronic state of low-grade inflammation that is exacerbated by the anatomical proximity of tumors to abdominal hypertrophic adipose depots, resulting in alterations of cancer-cell metabolism and biology, which are thought to promote CRC progression (51, 52, 56). Yet, surprisingly little is known about how altered lipid metabolism contributes to the aggressive evolution of CRC in obese patients. We find that, despite the remarkable genetic and phenotypic heterogeneity of CRC (57), CES1 expression markedly increases in the metastasis-prone mesenchymal CMS4 subtype and portends worse clinical outcomes in overweight/obese patients. It was previously suggested that cancer cells utilize fatty acids released by TME-based adipocytes and stromal cells to support rapid tumor growth (17, 58).

Our data do not exclude a role for this metabolic symbiosis between cancer and non-cancerous cells in CRC, nor an additional role for CES1 in tumor-associated adipocytes. However, our findings from the investigations of CRC patients and preclinical cellular and animal models underscore the importance of the cell-autonomous mechanism mediated by CES1 in mobilising FFAs from endogenous lipid reservoirs for supporting CRC-cell survival under energy stress conditions. Indeed, these endogenous FFAs would presumably represent the only source of FAO fuels available to CRC cells for maintaining metabolic homeostasis upon loss of attachment or migration outside the TME, during the initial stages of metastasis (15). By increasing FFA availability and oxidative energy metabolism, elevated CES1 expression could also link inflammation with the EMT in inflamed CMS4 tumors, in keeping with the roles of FAO and inflammation in both driving and maintaining stemness in cancer (15, 18).

The identification of actionable therapeutic targets that are linked to the pathogenesis of core molecular tumor subtypes is an area of major interest and clinical need, particularly in obesity-associated mesenchymal tumors, given their higher risk of metastasis, relapse, and resistance to cancer therapy (57). However, translating oncological metabolic targets to the clinical setting has been complicated by the frequent toxicities produced by the suppression of mechanisms that are also required for normal cell function (59, 60). Interestingly, in this regard, CES1 appears to be a promising therapeutic target in CRC, given its contextual specificity for energy stress conditions and its selective overactivation in microsatellite stable/non-hypermutated CMS4 (mesenchymal) and CMS2 tumors, which are generally refractory to immune-checkpoint blockade immunotherapy. Accordingly, as well as systemic pharmacologic inhibition, genetic *Ces1d* deletion appears to be well tolerated in mouse models, because *Ces1d* knockout mice are viable, lean and seemingly healthy (61). Indeed, the short half-life and poor stability of the tool compounds used in our study underscore the therapeutic potential of the CES1-dependent metabolic mechanism in CRC and need for developing novel CES1 inhibitors with improved bioavailability. Thus, while

further investigations will determine whether CES1 blockade can be developed into an effective treatment strategy in obese CRC patients, our findings may serve as an example for developing tumor subtype-based interventions that target core tumor-cell vulnerabilities also in cancers beyond CRC.

METHODS

A detailed discussion of the Methods is reported in the Supplementary Information.

SUPPLEMENTARY INFORMATION

The Supplementary Information includes Methods, seven Figures, two Tables and Supplementary References.

DATA AVAILABILITY

mRNAseq dataset generated in the current study (Figure 3A) is included in the Supplementary Information files as Supplementary Table 2 and has been submitted to the European Nucleotide Archive under accession number, PRJEB32382.

The Metabolic Profiling datasets (general platform and lipid platform) generated in the current study (Figure 1D-1E, Figure 2A, Figure 2C-2E, Figure 4A-4B, Figure 4D, Figure 6B, Figure S2A, Figure S4A) are included in the Supplementary Information files as Supplementary Table 1.

The Lipid Profiling dataset generated from CRC patients is available from the corresponding authors upon request.

Data from the analysis of The Cancer Genome Atlas (TCGA) CRC (COADREAD) program and the French National Cartes d'identité des Tumeurs (FNCIT) program were classified according to the CMS algorithms described by the Colorectal Cancer Subtyping Consortium (CRCSC) and downloaded using the Synapse browser (ID: syn2623706). Additional information is available in the section "CRC patients and human CRC datasets" of the Methods in the Supplementary Information files.

AUTHORS CONTRIBUTIONS

G.F. and D.C. conceived the project and designed the experiments. D.D.A. conceived and designed the bioinformatic analysis and performed the statistical analysis of the data. D.C., F.B., L.T., S.L., J.E., D.V., J.B., and L.S. contributed to performing and analysing the biological experiments. D.C., L.G, A.D.V., G.C. J.K.E., H.C.K. and K.B. conducted the metabolic analyses and processed and analysed the data. D.D.A., J.A., J.M. and M.L.D. performed the metabolic profiling of CRC patient samples and the analysis of the clinical data. S.M., Z.T. and J.K contributed CRC clinical samples and metabolic and clinical analyses of patient samples. T.S.V., Y.M., W.S., G. Frost and V.T. contributed key reagents and technical expertise. G.F., D.C. and D.D.A. wrote the manuscript. All authors read and edited the manuscript. D.C. and D.D.A. contributed equally to this work. D.C. is listed first because she initiated the project.

ACKNOWLEDGEMENTS

We thank Steven Ley, Jacques Behmoaras, Navdeep Chandel, Richard Lehner, David Carling and Antonio Iavarone for critical comments on the manuscript. We also thank Enrico De Smaele for the Tween lentiviral vector. This work was supported in part by Cancer Research UK programme grant A15115, Medical Research Council (MRC) Biomedical

Catalyst grant MR/L005069/1, Bloodwise project grant 15003, and NIHR Imperial Biomedical Research Centre (BRC) ITMAT Push for Impact award P81135 to G.F. Infrastructure support for this research was provided in part by the NIHR Imperial BRC. L.G., A.D.V and G.C. acknowledge the Università degli Studi di Perugia and MIUR for financial support to the project AMIS, through the program “Dipartimenti di Eccellenza 2018-2022”.

REFERENCES

1. Cairns RA, Harris IS, and Mak TW. Regulation of cancer cell metabolism. *Nat Rev Cancer*. 2011;11(2):85-95.
2. Pavlova NN, and Thompson CB. The Emerging Hallmarks of Cancer Metabolism. *Cell Metab*. 2016;23(1):27-47.
3. Boroughs LK, and DeBerardinis RJ. Metabolic pathways promoting cancer cell survival and growth. *Nat Cell Biol*. 2015;17(4):351-9.
4. Kreuzaler P, Panina Y, Segal J, and Yuneva M. Adapt and conquer: Metabolic flexibility in cancer growth, invasion and evasion. *Mol Metab*. 2019. 33:83-101.
5. Hirayama A, Kami K, Sugimoto M, Sugawara M, Toki N, Onozuka H, et al. Quantitative metabolome profiling of colon and stomach cancer microenvironment by capillary electrophoresis time-of-flight mass spectrometry. *Cancer Res*. 2009;69(11):4918-25.
6. Urasaki Y, Heath L, and Xu CW. Coupling of glucose deprivation with impaired histone H2B monoubiquitination in tumors. *PLoS One*. 2012;7(5):e36775.

7. Vander Heiden MG, and DeBerardinis RJ. Understanding the Intersections between Metabolism and Cancer Biology. *Cell*. 2017;168(4):657-69.
8. Yun J, Rago C, Cheong I, Pagliarini R, Angenendt P, Rajagopalan H, et al. Glucose deprivation contributes to the development of KRAS pathway mutations in tumor cells. *Science*. 2009;325(5947):1555-9.
9. Miyo M, Konno M, Nishida N, Sueda T, Noguchi K, Matsui H, et al. Metabolic Adaptation to Nutritional Stress in Human Colorectal Cancer. *Sci Rep*. 2016;6:38415.
10. Zhang M, Liu T, Sun H, Weng W, Zhang Q, Liu C, et al. Pim1 supports human colorectal cancer growth during glucose deprivation by enhancing the Warburg effect. *Cancer Sci*. 2018;109(5):1468-79.
11. Ma L, Tao Y, Duran A, Llado V, Galvez A, Barger JF, et al. Control of nutrient stress-induced metabolic reprogramming by PKCzeta in tumorigenesis. *Cell*. 2013;152(3):599-611.
12. Tang J, Yan T, Bao Y, Shen C, Yu C, Zhu X, et al. LncRNA GLCC1 promotes colorectal carcinogenesis and glucose metabolism by stabilizing c-Myc. *Nat Commun*. 2019;10(1):3499.
13. Sanchez-Martinez R, Cruz-Gil S, Gomez de Cedron M, Alvarez-Fernandez M, Vargas T, Molina S, et al. A link between lipid metabolism and epithelial-mesenchymal transition provides a target for colon cancer therapy. *Oncotarget*. 2015;6(36):38719-36.
14. Morandi A, Taddei ML, Chiarugi P, and Giannoni E. Targeting the Metabolic Reprogramming That Controls Epithelial-to-Mesenchymal Transition in Aggressive Tumors. *Front Oncol*. 2017;7:40.

15. Carracedo A, Cantley LC, and Pandolfi PP. Cancer metabolism: fatty acid oxidation in the limelight. *Nat Rev Cancer*. 2013;13(4):227-32.
16. Wang YN, Zeng ZL, Lu J, Wang Y, Liu ZX, He MM, et al. CPT1A-mediated fatty acid oxidation promotes colorectal cancer cell metastasis by inhibiting anoikis. *Oncogene*. 2018;37(46):6025-40.
17. Wen YA, Xing X, Harris JW, Zaytseva YY, Mitov MI, Napier DL, et al. Adipocytes activate mitochondrial fatty acid oxidation and autophagy to promote tumor growth in colon cancer. *Cell Death Dis*. 2017;8(2):e2593.
18. Taniguchi K, and Karin M. NF-kappaB, inflammation, immunity and cancer: coming of age. *Nat Rev Immunol*. 2018;18(5):309-24.
19. DiDonato JA, Mercurio F, and Karin M. NF-kappa B and the link between inflammation and cancer. *Immunol Rev*. 2012;246:379-400.
20. Schwitalla S, Fingerle AA, Cammareri P, Nebelsiek T, Goktuna SI, Ziegler PK, et al. Intestinal tumorigenesis initiated by dedifferentiation and acquisition of stem-cell-like properties. *Cell*. 2013;152(1-2):25-38.
21. Greten FR, Eckmann L, Greten TF, Park JM, Li ZW, Egan LJ, et al. IKKbeta links inflammation and tumorigenesis in a mouse model of colitis-associated cancer. *Cell*. 2004;118(3):285-96.
22. Ishak Gabra MB, Yang Y, Lowman XH, Reid MA, Tran TQ, and Kong M. IKKbeta activates p53 to promote cancer cell adaptation to glutamine deprivation. *Oncogenesis*. 2018;7(11):93.
23. Wang X, Liu R, Qu X, Yu H, Chu H, Zhang Y, et al. alpha-Ketoglutarate-Activated NF-kappaB Signaling Promotes Compensatory Glucose Uptake and Brain Tumor Development. *Mol Cell*. 2019;76(1):148-62 e7.

24. Mauro C, Leow SC, Anso E, Rocha S, Thotakura AK, Tornatore L, et al. NF-kappaB controls energy homeostasis and metabolic adaptation by upregulating mitochondrial respiration. *Nat Cell Biol.* 2011;13(10):1272-9.
25. Maedera S, Mizuno T, Ishiguro H, Ito T, Soga T, and Kusuhara H. GLUT6 is a lysosomal transporter that is regulated by inflammatory stimuli and modulates glycolysis in macrophages. *FEBS Lett.* 2019;593(2):195-208.
26. Bhat KPL, Balasubramaniyan V, Vaillant B, Ezhilarasan R, Hummelink K, Hollingsworth F, et al. Mesenchymal differentiation mediated by NF-kappaB promotes radiation resistance in glioblastoma. *Cancer Cell.* 2013;24(3):331-46.
27. Wu Y, Deng J, Rychahou PG, Qiu S, Evers BM, and Zhou BP. Stabilization of snail by NF-kappaB is required for inflammation-induced cell migration and invasion. *Cancer Cell.* 2009;15(5):416-28.
28. Tornatore L, Thotakura AK, Bennett J, Moretti M, and Franzoso G. The nuclear factor kappa B signaling pathway: integrating metabolism with inflammation. *Trends Cell Biol.* 2012;22(11):557-66.
29. Patel M, Horgan PG, McMillan DC, and Edwards J. NF-kappaB pathways in the development and progression of colorectal cancer. *Transl Res.* 2018;197:43-56.
30. Kojima M, Morisaki T, Sasaki N, Nakano K, Mibu R, Tanaka M, et al. Increased nuclear factor-kB activation in human colorectal carcinoma and its correlation with tumor progression. *Anticancer Res.* 2004;24(2B):675-81.
31. Moorchung N, Kunwar S, and Ahmed KW. An evaluation of nuclear factor kappa B expression in colorectal carcinoma: an analysis of 50 cases. *J Cancer Res Ther.* 2014;10(3):631-5.

32. Wu D, Wu P, Zhao L, Huang L, Zhang Z, Zhao S, et al. NF-kappaB Expression and Outcomes in Solid Tumors: A Systematic Review and Meta-Analysis. *Medicine (Baltimore)*. 2015;94(40):e1687.
33. Guinney J, Dienstmann R, Wang X, de Reynies A, Schlicker A, Soneson C, et al. The consensus molecular subtypes of colorectal cancer. *Nat Med*. 2015;21(11):1350-6.
34. Hayden MS, and Ghosh S. Signaling to NF-kappaB. *Genes Dev*. 2004;18(18):2195-224.
35. Goracci L, Tortorella S, Tiberi P, Pellegrino RM, Di Veroli A, Valeri A, et al. Lipostar, a Comprehensive Platform-Neutral Cheminformatics Tool for Lipidomics. *Anal Chem*. 2017;89(11):6257-64.
36. Luo JL, Kamata H, and Karin M. IKK/NF-kappaB signaling: balancing life and death--a new approach to cancer therapy. *J Clin Invest*. 2005;115(10):2625-32.
37. Birsoy K, Possemato R, Lorbeer FK, Bayraktar EC, Thiru P, Yucel B, et al. Metabolic determinants of cancer cell sensitivity to glucose limitation and biguanides. *Nature*. 2014;508(7494):108-12.
38. Rambold AS, Cohen S, and Lippincott-Schwartz J. Fatty acid trafficking in starved cells: regulation by lipid droplet lipolysis, autophagy, and mitochondrial fusion dynamics. *Dev Cell*. 2015;32(6):678-92.
39. Zhang L, and Romero P. Metabolic Control of CD8(+) T Cell Fate Decisions and Antitumor Immunity. *Trends Mol Med*. 2018;24(1):30-48.
40. Lian J, Nelson R, and Lehner R. Carboxylesterases in lipid metabolism: from mouse to human. *Protein Cell*. 2018;9(2):178-95.

41. Dominguez E, Galmozzi A, Chang JW, Hsu KL, Pawlak J, Li W, et al. Integrated phenotypic and activity-based profiling links *Ces3* to obesity and diabetes. *Nat Chem Biol.* 2014;10(2):113-21.
42. Gilham D, Ho S, Rasouli M, Martres P, Vance DE, and Lehner R. Inhibitors of hepatic microsomal triacylglycerol hydrolase decrease very low density lipoprotein secretion. *FASEB J.* 2003;17(12):1685-7.
43. Aflaki E, Radovic B, Chandak PG, Kolb D, Eisenberg T, Ring J, et al. Triacylglycerol accumulation activates the mitochondrial apoptosis pathway in macrophages. *J Biol Chem.* 2011;286(9):7418-28.
44. Galluzzi L, Vitale I, Aaronson SA, Abrams JM, Adam D, Agostinis P, et al. Molecular mechanisms of cell death: recommendations of the Nomenclature Committee on Cell Death 2018. *Cell Death Differ.* 2018;25(3):486-541.
45. Yang WS, and Stockwell BR. Ferroptosis: Death by Lipid Peroxidation. *Trends Cell Biol.* 2016;26(3):165-76.
46. Stockwell BR, Friedmann Angeli JP, Bayir H, Bush AI, Conrad M, Dixon SJ, et al. Ferroptosis: A Regulated Cell Death Nexus Linking Metabolism, Redox Biology, and Disease. *Cell.* 2017;171(2):273-285
47. Feng H, Stockwell BR. Unsolved mysteries: How does lipid peroxidation cause ferroptosis?. *PLoS Biol.* 2018;16(5):e2006203.
48. Yang WS, SriRamaratnam R, Welsch ME, Shimada K, Skouta R, Viswanathan VS et al. Regulation of ferroptotic cancer cell death by GPX4. *Cell.* 2014;156(1-2):317-331.
49. Cancer Genome Atlas N. Comprehensive molecular characterization of human colon and rectal cancer. *Nature.* 2012;487(7407):330-7.

50. Calle EE, Rodriguez C, Walker-Thurmond K, and Thun MJ. Overweight, obesity, and mortality from cancer in a prospectively studied cohort of U.S. adults. *N Engl J Med*. 2003;348(17):1625-38.
51. O'Keefe SJD. Diet, microorganisms and their metabolites, and colon cancer. *Nat Rev Gastro Hepat*. 2016;13(12):691-706.
52. Park J, Morley TS, Kim M, Clegg DJ, and Scherer PE. Obesity and cancer--mechanisms underlying tumour progression and recurrence. *Nat Rev Endocrinol*. 2014;10(8):455-65.
53. Wang H, Liang L, Fang JY, and Xu J. Somatic gene copy number alterations in colorectal cancer: new quest for cancer drivers and biomarkers. *Oncogene*. 2016;35(16):2011-9.
54. Xu J, Xu Y, Li Y, Jadhav K, You M, Yin L, et al. Carboxylesterase 1 Is Regulated by Hepatocyte Nuclear Factor 4alpha and Protects Against Alcohol- and MCD diet-induced Liver Injury. *Sci Rep*. 2016;6:24277.
55. Huang J, Li L, Lian J, Schauer S, Vesely PW, Kratky D, et al. Tumor-Induced Hyperlipidemia Contributes to Tumor Growth. *Cell Rep*. 2016;15(2):336-48.
56. Nieman KM, Romero IL, Van Houten B, and Lengyel E. Adipose tissue and adipocytes support tumorigenesis and metastasis. *Biochim Biophys Acta*. 2013;1831(10):1533-41.
57. Dienstmann R, Vermeulen L, Guinney J, Kopetz S, Tejpar S, and Tabernero J. Consensus molecular subtypes and the evolution of precision medicine in colorectal cancer. *Nat Rev Cancer*. 2017;17(4):268.

58. Nieman KM, Kenny HA, Penicka CV, Ladanyi A, Buell-Gutbrod R, Zillhardt MR, et al. Adipocytes promote ovarian cancer metastasis and provide energy for rapid tumor growth. *Nat Med.* 2011;17(11):1498-503.
59. Counihan JL, Grossman EA, and Nomura DK. Cancer Metabolism: Current Understanding and Therapies. *Chem Rev.* 2018;118(14):6893-923.
60. DeBerardinis RJ, and Chandel NS. Fundamentals of cancer metabolism. *Sci Adv.* 2016;2(5):e1600200.
61. Wei E, Ben Ali Y, Lyon J, Wang H, Nelson R, Dolinsky VW, et al. Loss of TGH/Ces3 in mice decreases blood lipids, improves glucose tolerance, and increases energy expenditure. *Cell Metab.* 2010;11(3):183-93.

FIGURES AND FIGURE LEGENDS

FIGURE 1

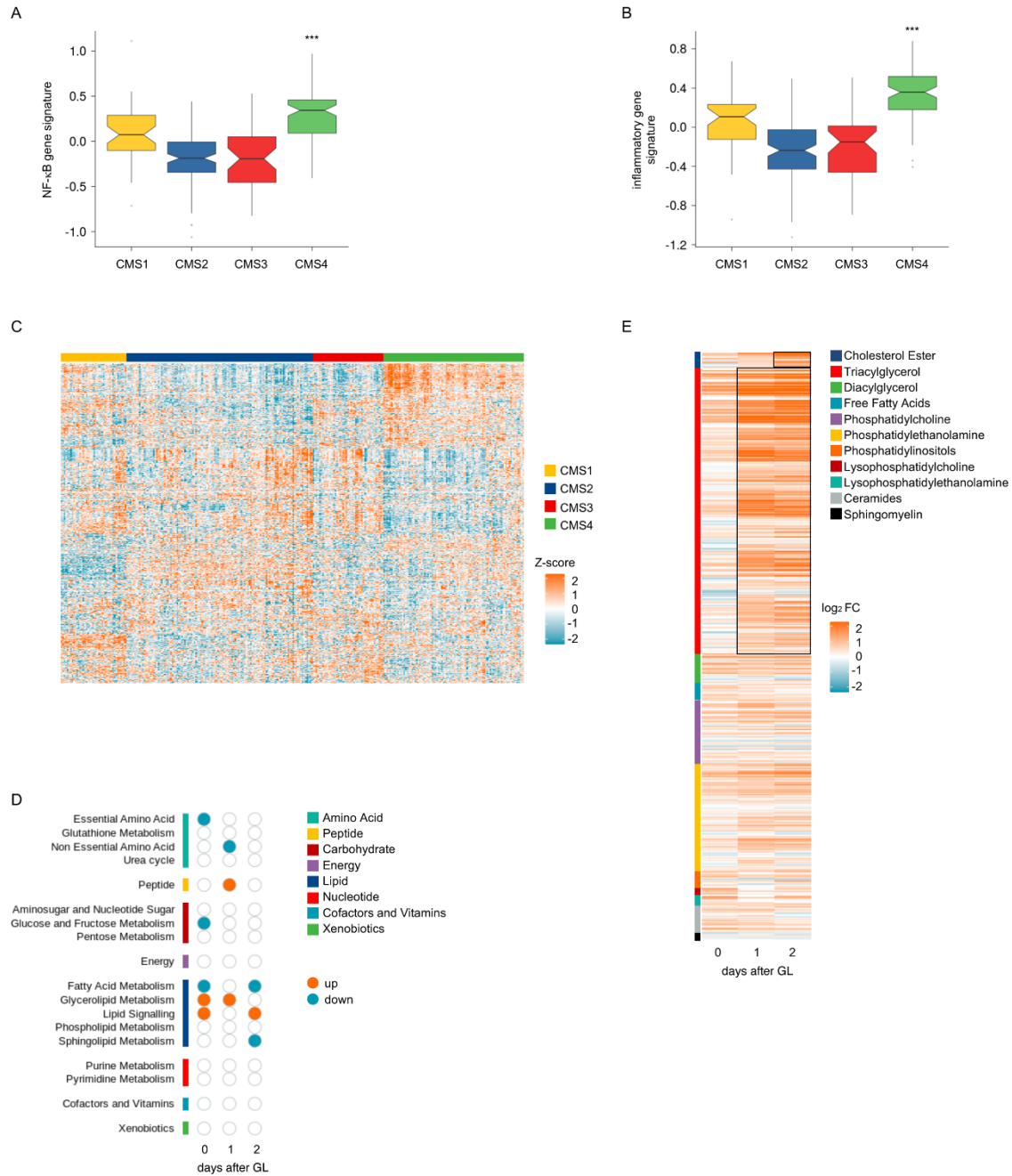


FIGURE 1. NF- κ B is activated in the mesenchymal CMS4 CRC subtype and regulates lipid metabolism upon starvation

A-B, Boxplots showing the median Z-scores of the NF- κ B-activation (**A**) and inflammatory (**B**)-gene signatures in each CMS subtype from CRC patients (n=296) in The Cancer Genome Atlas (TCGA) dataset. Shown in the boxplots are the median values (horizontal lines), 25th-75th percentiles (box outlines), and highest and lowest values within 1.5x of the inter-quartile range (vertical lines). Notches denote the 95% confidence interval of the medians. Samples from each CMS subtype were compared to other CRC samples by using two-tailed Student's t-test. ***, $p < 0.001$. Statistical significance for multiple comparisons was calculated using the Kruskal-Wallis test ($p < 2.2 \times 10^{-16}$).

C, Hierarchical clustering of the 1,795 metabolic genes present in the Reactome database from the patients in (**A-B**), arranged according to CMS subtype. The Z-scores of gene expression are depicted as a gradient from azure (low expression) to orange (high expression). Yellow, CMS1; blue, CMS2; red, CMS3; green, CMS4.

D, Metabolite set enrichment analysis of significantly deregulated biochemicals ($q < 0.05$) in MEFs expressing RelA-specific (RelA) relative to non-specific (ns) shRNAs (n=5), cultured under normal conditions (0) or for the indicated times under GL. p values were corrected using the Benjamini-Hochberg false-discovery rate (FDR) procedure. Orange, over-enrichment (up); azure, under-enrichment (down).

E, Heatmap showing the \log_2 fold change of metabolic species in the indicated lipid classes in RelA-deficient relative to control MEFs treated as in (**D**). Shown are the lipid species having a value different from zero in at least one of the time points investigated. Orange, increased abundance; azure, decreased abundance. Framed in black are the lipid classes showing statistically significant accumulation, as determined by a hypergeometric test, corrected using the Benjamini-Hochberg procedure (Cholesterol Ester: d2, $q = 4.55e^{-2}$; Triacylglycerol: d1, $q = 4.44e^{-7}$; d2, $q = 1.19e^{-5}$).

D, E Metabolic analysis were conducted at Metabolon (Morrisville, NC).

FIGURE 2

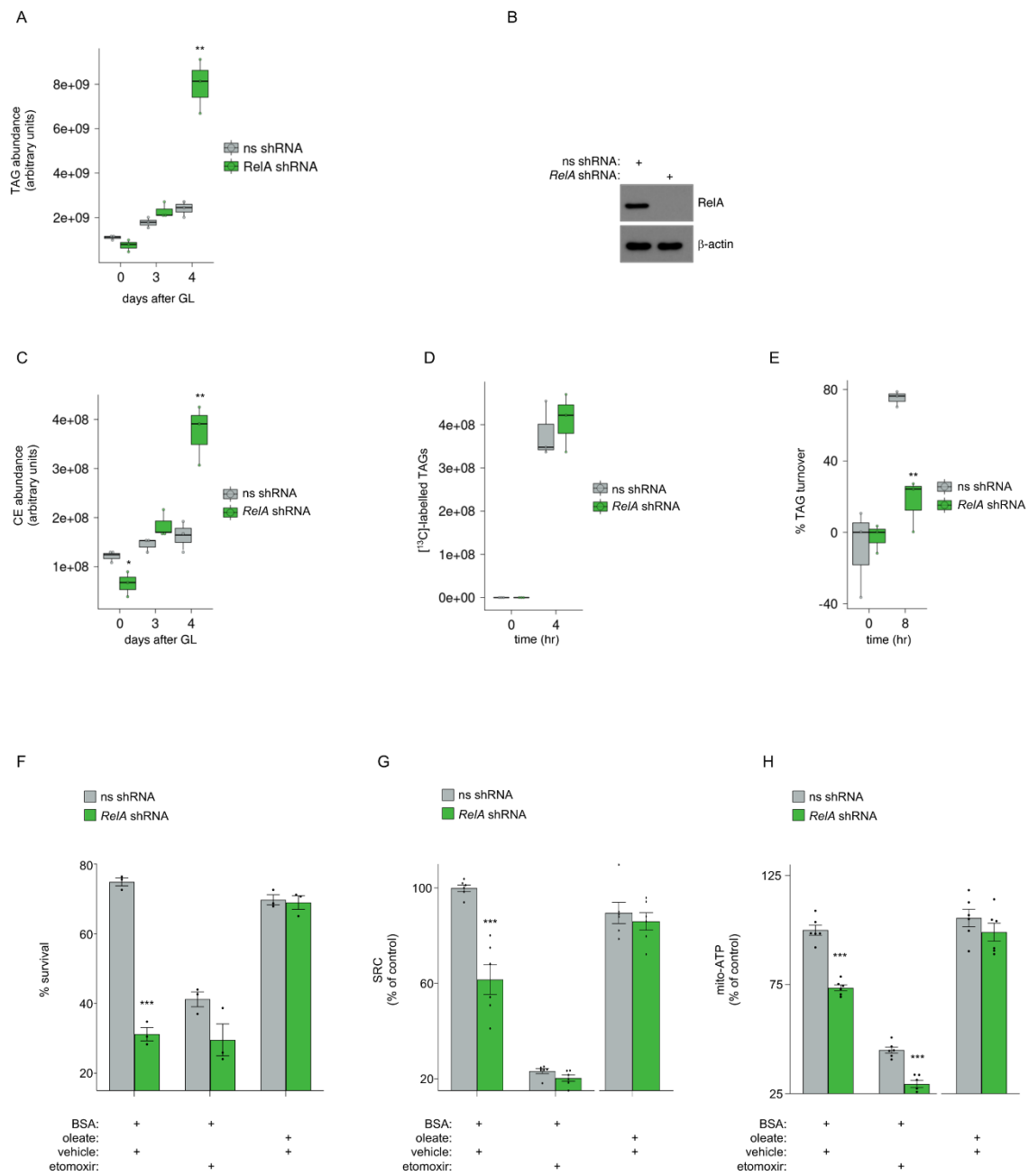


FIGURE 2. NF-κB inhibition impairs oxidative FFA metabolism and CRC-cell survival during starvation

A, Boxplots showing the relative TAG abundance (n=80) in CT-26 cells expressing RelA-specific versus ns shRNAs and cultured under normal (0) or GL conditions, as shown. The relative TAG abundance was derived by adding the peak area for each TAG, identified by LC-MS and Lipostar software (Molecular Discovery Ltd, UK).

B, Western blots showing RelA and β -actin protein levels in CT-26 cells from (**A**).

C, Boxplots showing the relative CE abundance (n=16) in CT-26 cells from (**A**) during GL. The relative CE abundance was derived by adding the peak area for each CE, identified as in (**A**).

D, Boxplots showing the relative abundance of [^{13}C]-labelled TAGs (n=7), determined by LC-MS flux analysis and Lipostar software in CT-26 cells expressing RelA-specific or ns shRNAs, before or after [^{13}C]-oleate addition in the presence of E600 and etomoxir.

E, Boxplots showing the TAG turnover calculated as in (**D**), using [^{13}C]-oleate, in CT-26 cells expressing RelA-specific or ns shRNAs as in (**A**). TAG turnover reports the percentage of decrease of [^{13}C]-labelled TAG abundance (n=40) at 8 relative to 0 hr, in the presence of triacsin C and forskolin.

F, Trypan blue exclusion assays showing the percentage of live CT-26 cells expressing RelA-specific or ns shRNAs as in (**A**) after 4 days under GL, in the presence of the indicated treatments. Values denote means \pm SD (n=3).

G, SRC measured by Seahorse in cells from (**A**), treated as shown.

H, Mitochondrial ATP production rate (mito-ATP) measured by Seahorse in cells from (**A**), treated as shown.

A, C-E, Shown in the boxplots are the medians (horizontal lines), 25th-75th percentiles (box outlines), and highest and lowest values within 1.5x of the inter-quartile range (vertical lines).

F-H, BSA and BSA-oleate, 200 μM .

F-G, Etomoxir, 10 μM .

G-H, Means report the percentages of the control values \pm SEM (n=6).

B, F-H, Experiments were conducted at least three times.

A, C-H, Statistical significance was calculated by two-tailed Student's t-test. *, $p < 0.05$; **, $p < 0.01$; ***, $p < 0.001$.

FIGURE 3

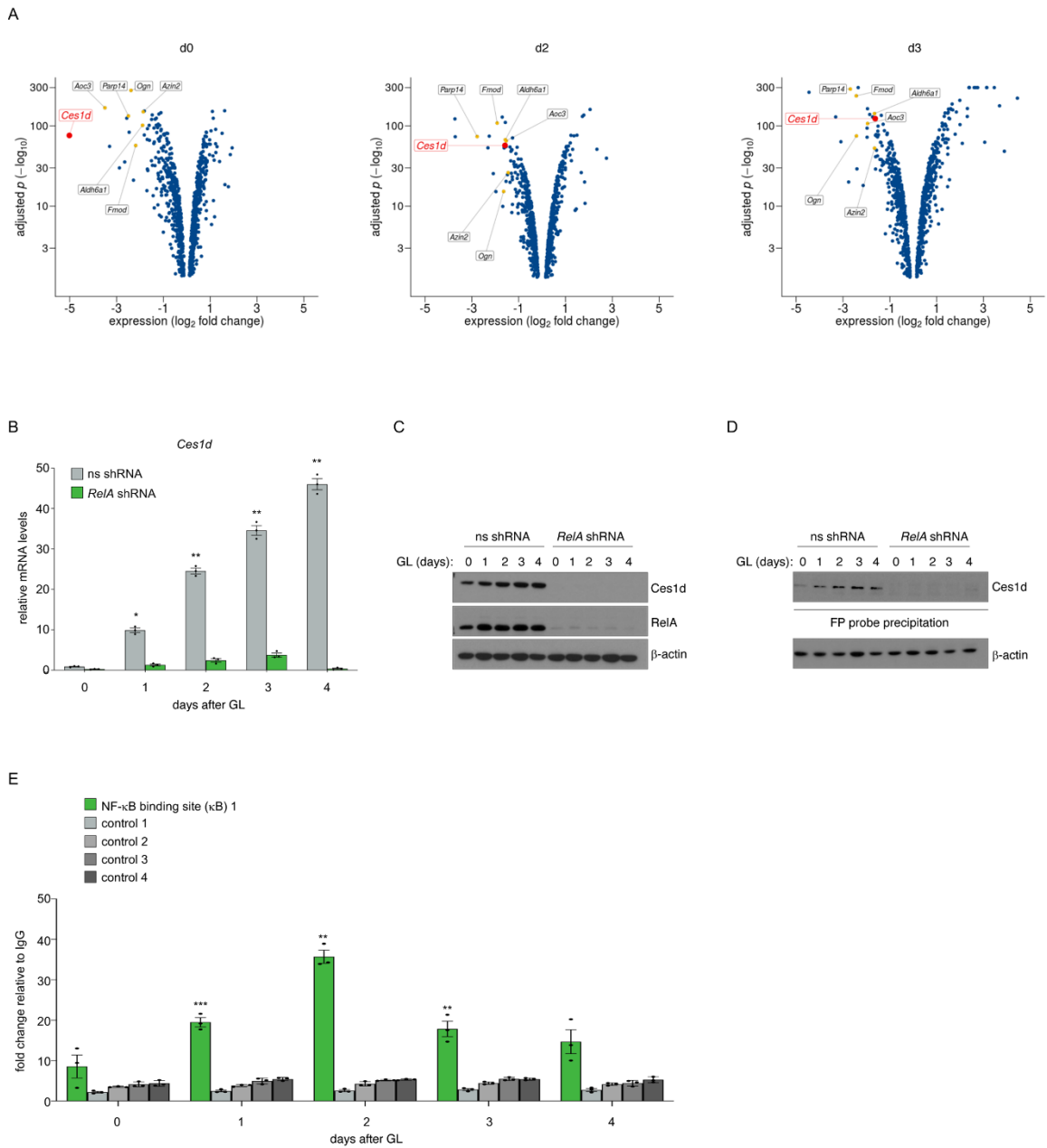


FIGURE 3. *Ces1d* is a direct transcriptional target of NF-κB and one of the top seven genes upregulated by NF-κB during starvation

A, Volcano plots showing differentially expressed metabolic genes ($q < 0.05$; d0, n=801; d2, n=726; d3, n=833) in RelA-deficient relative to control MEFs (n=5) cultured under normal conditions (d0) or for two (d2) or three (d3) days under GL. Reported are the negative \log_{10} transformed adjusted p values plotted against the average \log_2 fold changes. Dots represent individual genes. *Ces1d* is depicted as a red dot; the other six most markedly downregulated metabolic genes in RelA-deficient relative to control MEFs, across all time points investigated, are depicted as orange dots.

B, qRT-PCR showing the *Ces1d* mRNA levels in CT-26 cells expressing RelA-specific or ns shRNAs and cultured under normal conditions (0) or for the indicated times under GL. Values denote means \pm SD (n=3).

C, Western blots showing the protein levels of *Ces1d*, RelA and β -actin in CT-26 cells from **(B)**.

D, Desthiobiotin-fluorophosphonate activity-based (FP) probe precipitation assays showing the *Ces1d*-specific serine esterase activity in CT-26 cells from **(B)**, as determined by streptavidin-mediated precipitation of the biotin-bound FP probe followed by western blots with anti-*Ces1d* antibody. β -actin in the total cell lysates (input) used for the activity-based protein profile (ABPP) assay is shown as a loading control.

E, Chromatin immunoprecipitation assays showing the binding of NF- κ B/RelA complexes to κ B DNA element (κ B)1 in the promoter region of *Ces1d* or the indicated control DNA regions (controls 1-4) in CT-26 cells from **(B)**. Values denote means \pm SEM (n=3).

B-E, Experiments were conducted at least three times.

B, E, Statistical significance was calculated by two-tailed Student's t-test. *, $p < 0.05$; **, $p < 0.01$; ***, $p < 0.001$.

FIGURE 4

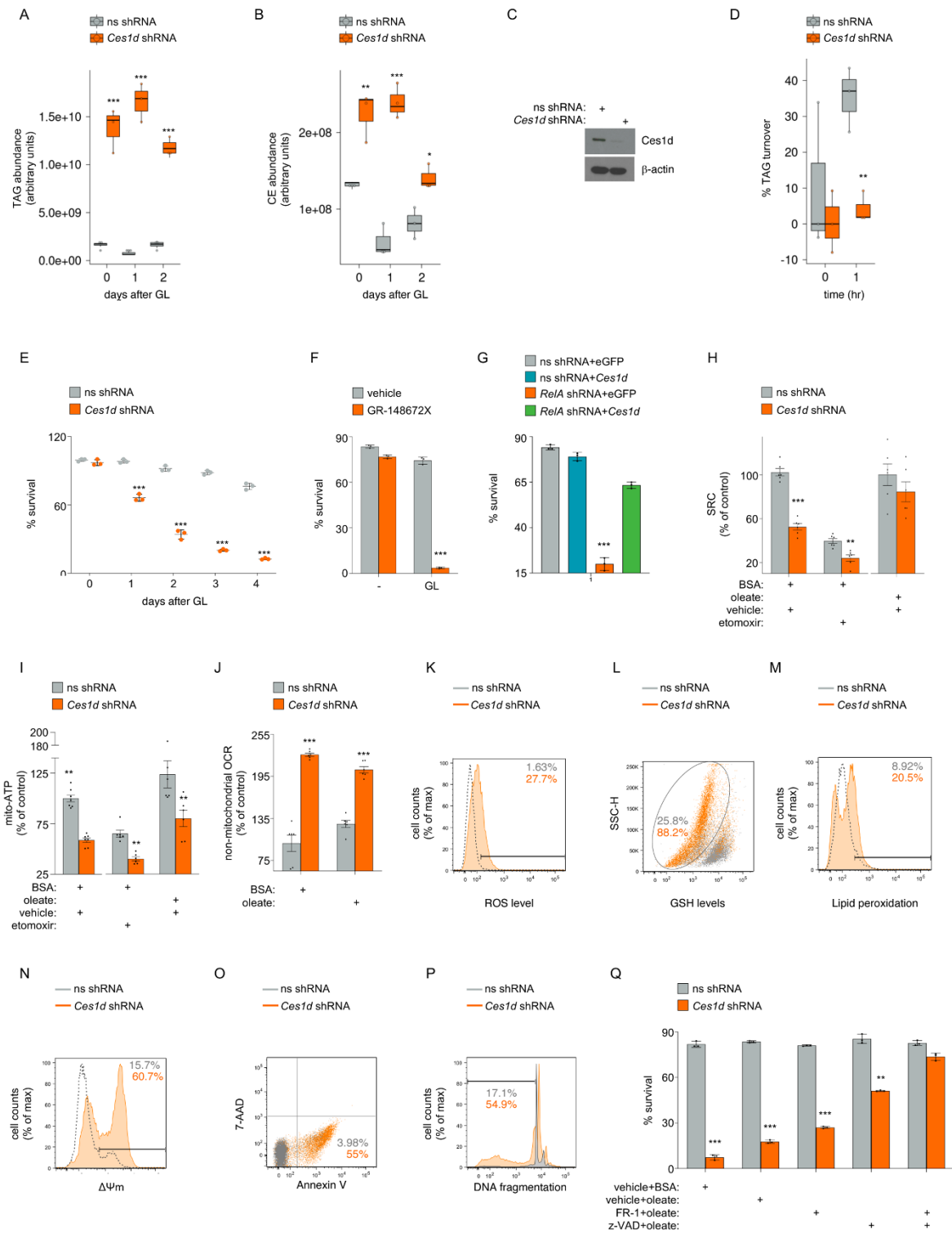


FIGURE 4. *Ces1d* mediates NF- κ B-dependent metabolic adaptation by enhancing oxidative FFA catabolism and preventing toxic TAG accumulation

- A**, Boxplots showing the relative TAG abundance (n=92) in CT-26 cells expressing Ces1d-specific (Ces1d) or ns shRNAs and cultured under normal (0) or GL conditions. Relative TAG abundance was derived as in Figure 2A.
- B**, Boxplots showing the relative CE abundance (n=9) in cells from (**A**) during GL. Relative CE abundance was derived as in Figure 2C.
- C**, Western blots showing Ces1d and β -actin protein levels in cells from (**A**).
- D**, Boxplots showing TAG turnover, calculated as in Figure 2E, in CT-26 cells expressing Ces1d-specific or ns shRNAs as in (**A**). TAG turnover reports the percentage of decrease of [^{13}C]-labelled TAG abundance (n=40) at 1 relative to 0 hr in the presence of triacsin C and forskolin as in Figure 2E.
- E**, Trypan blue exclusion assays showing the percentage of live CT-26 cells expressing Ces1d-specific or ns shRNAs as in (**A**) during GL.
- F**, Trypan blue exclusion assays showing the percentage of live CT-26 cells after a 4-day treatment with GR-148672X (10 μM) or vehicle under normal (-) or GL conditions.
- G**, Trypan blue exclusion assays showing the percentage of live RelA deficient (RelA) or control (ns) CT-26 cells expressing eGFP or Ces1d after a 4-day culture under GL.
- H**, SRC measured by Seahorse in CT-26 cells from (**A**). Etomoxir, 10 μM .
- I**, Mito-ATP measured by Seahorse in CT-26 cells from (**A**), treated as shown.
- J**, Non-mitochondrial OCR measured by Seahorse in CT-26 cells from (**A**), treated as shown (n=5).
- K**, FACS analysis showing ROS levels in CT-26 cells from (**A**) after a 3-day culture under GL.

L, FACS analysis showing GSH levels in CT-26 cells from (**A**) after a 4-day culture under GL.

M, FACS analysis showing the lipid peroxidation in CT-26 cells from (**A**) after a 4-day culture under GL.

N, FACS analysis showing the percentage of CT-26 cells from (**A**) stained with annexin V after a 2-day culture under GL.

O, Propidium iodide (PI) staining showing apoptotic CT-26 cells (*i.e.*, exhibiting sub-G₁ DNA content) in representative cultures from (**A**) after a 4-day culture under GL.

P, FACS analysis showing the loss of mitochondrial membrane potential ($\Delta\Psi_m$) in CT-26 cells from (**A**) after a 3-day culture under GL.

Q, Trypan blue exclusion assays showing the percentage of live CT-26 cells from (**A**) after a 4-day culture under GL in the presence of the indicated treatments. z-VAD-fmk, 50 μ M; Ferrostatin-1 (FR-1), 0.5 μ M.

A-B, D, Shown in the boxplots are the medians (horizontal lines), 25th-75th percentiles (box outlines), and highest and lowest values within 1.5x of the inter-quartile range (vertical lines).

E-F, Q, Values denote means \pm SD (n=3).

H-J, Means express the percentages of the control values \pm SEM (n=6).

H-J, Q, BSA and BSA-oleate, 200 μ M.

C, E-Q, Experiments were conducted at least three times.

A-B, D-J, Q, Statistical significance was calculated by two-tailed Student's t-test. *, $p < 0.05$; **, $p < 0.01$; ***, $p < 0.001$.

FIGURE 5

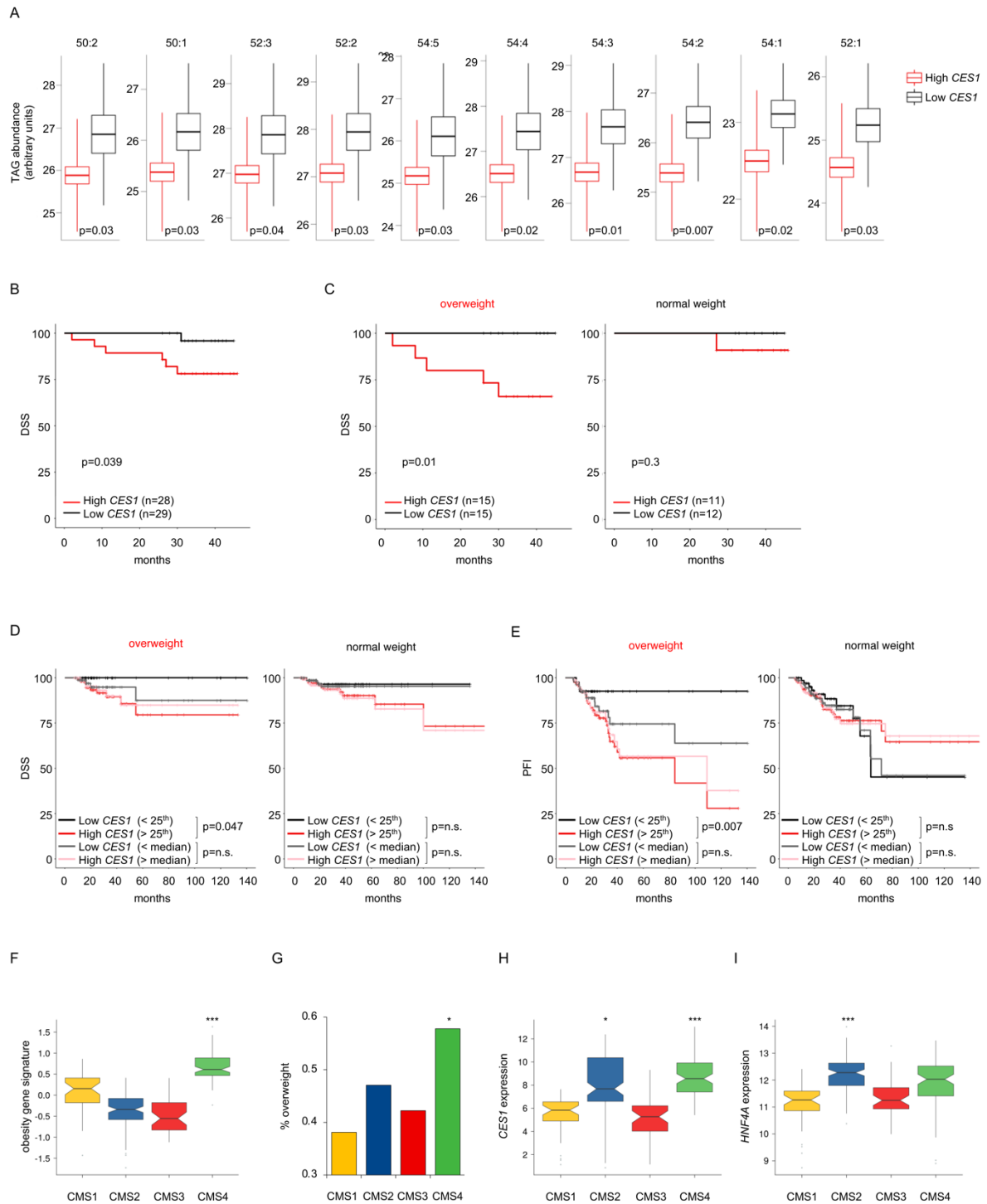


FIGURE 5. CES1 is selectively upregulated in CMS2 and CMS4 CRCs and denotes aggressive disease in obese/overweight patients

A, Boxplots showing TAG abundance in human CRCs (n=57) stratified based on *CES1* expression, assessed by qRT-PCR. Shown in the boxplots are the means (horizontal lines), means \pm SEM (box outlines) or \pm SD (vertical lines). Statistical significance was calculated by two-tailed Student's t-test.

B, DSS in CRC patients from (**A**) stratified based on tumor-associated *CES1* expression, assessed by qRT-PCR.

C, DSS in obese/overweight (left; n=30) and normal weight (right; n=23) CRC patients from (**A**) stratified based on *CES1* expression as in (**B**).

D, DSS in obese/overweight (left; n=157) and normal weight (right; n=272) CRC patients from the TCGA dataset (n=427) stratified based on tumor-associated *CES1* expression using the 25th or 50th percentile as stratification threshold.

E, PFI in obese/overweight (left; n=161) and normal weight (right; n=275) CRC patients from (**D**) stratified based on *CES1* expression as in (**D**).

F, Boxplots showing the median Z-scores of the obesity-gene signatures in each CMS CRC subtype from Figure 1A-1B.

G, Percentage of overweight CRC patients in CMS subtypes from the TCGA dataset (n=296). Samples from obese/overweight and normal weight patients in each subtype were compared to all other CRC samples using Fisher's exact test. *, $p=0.03$.

H-I, Boxplots showing *CES1* (**H**) and *HNF4A* (**I**) mRNA expression in CMS CRC subtypes (n=296) from patients in the TCGA dataset (**D**).

A-E, p values are indicated.

B-E, Statistical significance was calculated using the log-rank test.

F, H-I, Shown in the boxplots are the medians (horizontal lines), 25th-75th percentiles (box outlines), and highest and lowest values within 1.5x of the inter-quartile range (vertical lines). Notches denote the 95% confidence interval of the medians. Samples from each CMS subtype were compared to all other CRC samples using two-tailed Student's t-test. Statistical significance for multiple comparisons was calculated using the Kruskal-Wallis test ($p < 2.2 \times 10^{-16}$). *, $p < 0.05$; ***, $p < 0.001$.

FIGURE 6



FIGURE 6. CES1-dependent metabolic adaptation is reciprocally controlled by NF- κ B and HNF4 α in distinct CRCs

A, qRT-PCR showing *CES1* mRNA expression in the indicated human CRC cell lines expressing *RELA*-specific (*RELA*) or ns shRNAs.

B, Heatmap showing the \log_2 fold change of metabolic species in the indicated lipid classes in *RELA*-deficient (*RELA*) relative to control cells in the indicated human CRC cell lines, cultured under normal conditions (0) or GL for 4 days, identified by LC-MS and Lipostar software. Shown are the lipids having a value different from zero at the time points investigated. Orange, increased abundance; azure, decreased abundance. Statistical significance of the lipid accumulation during GL was determined by a hypergeometric test, corrected using the Benjamini-Hochberg procedure (Triacylglycerols in RKO cells at d4, $q = 5.47e-32$).

C, Trypan blue exclusion assays showing the percentage of live cells from the indicated human CRC cell lines expressing *CES1*-specific (*CES1*) or ns shRNAs after a 4-day culture under GL (top). Western blots showing *CES1* and β -actin protein levels in the same cells (bottom).

D, qRT-PCR showing the *CES1* mRNA expression in the human CRC cell lines from (**A**) expressing HNF4A-specific (*HNF4A*) or ns shRNAs.

E, Trypan blue exclusion assays showing the percentage of live cells from the indicated human CRC cell lines after a 4-day treatment with GR-148672X (10 μ M) or vehicle during GL (top). Values denote means \pm SD (n=3). Images of representative cells (bottom). Scale bar, 50 μ m.

A, D, Experiments were conducted twice.

C, E, Experiments were conducted at least three times.

A, C-E, Values denote means \pm SD (n=3). Statistical significance was calculated by two-tailed Student's t-test. **, $p < 0.01$; ***, $p < 0.001$.

FIGURE 7

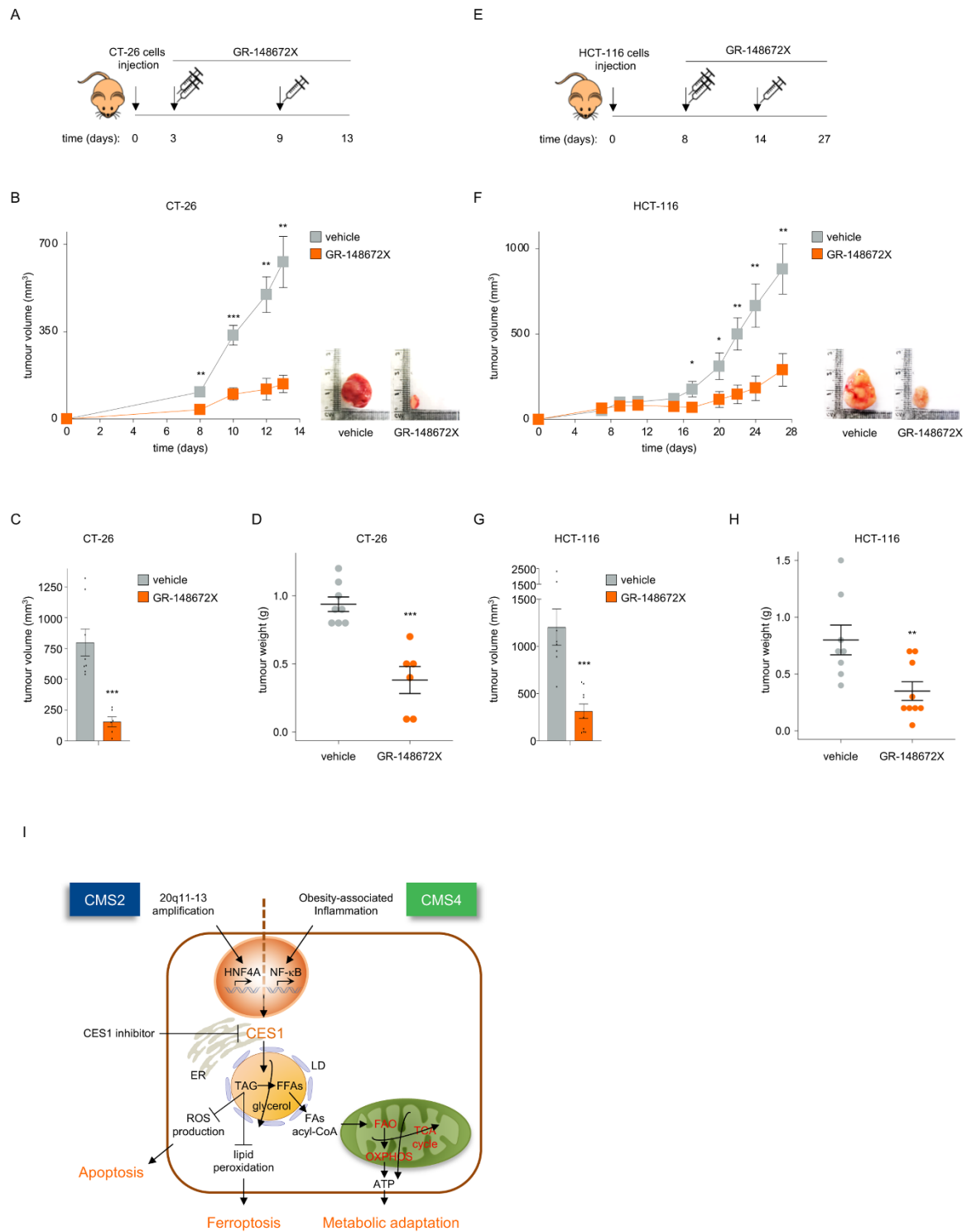


FIGURE 7. Pharmacologic Ces1d/CES1 inhibition counters CRC tumorigenesis in vivo

A, Diagram summarising the treatment schedule used in **(B)**.

B, Volumes of subcutaneous CT-26 CRC allografts in mice treated by intraperitoneal injection of GR-148672X (50 mg/kg) or vehicle as shown (left). Images of representative tumors isolated from mice at day 13 (right).

C, Volumes of subcutaneous CT-26 CRC tumours from **(B)** measured *ex vivo* at day 13.

D, Dot plots showing the weight of tumors from the mice in **(B)** at day 13.

E, Diagram summarising the treatment schedule used in **(F)**.

F, Volumes of subcutaneous HCT-116 CRC xenografts in mice treated by intraperitoneal injection of GR-148672X (50 mg/kg) or vehicle as shown (left). Images of representative tumors isolated from mice at day 27 (right).

G, Volumes of subcutaneous HCT-116 CRC tumours from **(F)** measured *ex vivo* at day 27.

H, Dot plots showing the weight of tumors from the mice in **(F)** at day 27.

I, Schematic representation of the reciprocal regulation of CES1 expression by NF- κ B and HNF4A in the CMS4 and CMS2 CRC subtypes, respectively. Depicted is the CES1-mediated metabolic mechanism increasing TAG breakdown to fuel FAO and OXPHOS during starvation, while preventing the toxic build-up of neutral lipids that triggers apoptosis and ferroptosis. ER, endoplasmic reticulum; LD, lipid droplet.

B-D, F-H, Values denote means \pm SEM.

B-D, GR-148672X-treated mice, n=6; vehicle-treated mice, n=8.

F-H, GR-148672X-treated mice, n=9; vehicle treated mice, n=8.

D, H, Horizontal lines and whiskers denote medians \pm SEM.

B-D, F-H, Statistical significance was calculated by two-tailed Student's t-test. *, $p < 0.05$; **, $p < 0.01$; ***, $p < 0.001$.